THE JOURNAL OF PHYSICAL CHEMISTRY C

Article

Cite This: J. Phys. Chem. C 2018, 122, 16113−16121

pubs.acs.org/JPCC

Biohybridization of Supported Gold Nanoassemblies on Silicon

Fatemeh Rahnemaye Rahsepar*,†,‡,# and Kam Tong Leung*,‡,#

†School of Chemistry, College of Science, University of Tehran, Tehran, Iran

‡WATLab and Department of Chemistry, University of Waterloo, Waterloo, Ontario N2L 3G1, Canada

Supporting Information

ABSTRACT: Understanding the molecular interactions of bio-organic molecules with metal nanoassemblies on a semiconductor surface is important to developing potential applications involving hybrid bio-organic metal interfaces. Here, we provide the first study of room-temperature growth evolution of L-cysteine on three notable Au nanoassemblies supported on the Si(111)7×7 surface. Our results indicate unidentate and/or bidentate arrangement of adsorbed cysteine on the Si substrate through Si−N and/or Si−S linkages, while in coexistence with the supported Au monomers and dimers. Similar to thiol-containing molecules adsorbed on other noble metals, cysteine chemisorbs via the S atom in neutral form on the supported Au nanocrystallite film. On the supported gold honeycomb nanonetwork, cysteine undergoes unidentate chemisorption through the thiol group with Au atoms and through the amino group with Si adatoms, which enables the remaining free functional groups to selectively bond with different incoming molecules. Instead of the "universal" three-stage growth found for cysteine adsorption on a pristine Si(111)7×7 surface, we observe the two-stage growth of cysteine on the supported gold honeycomb nanonetwork (i.e., without a transitional layer), similar to that found on a gold single-crystal surface. The formation of the ultrathin gold-silicide layer (honeycomb) has effectively transformed the semiconductor surface to a metal-like surface.

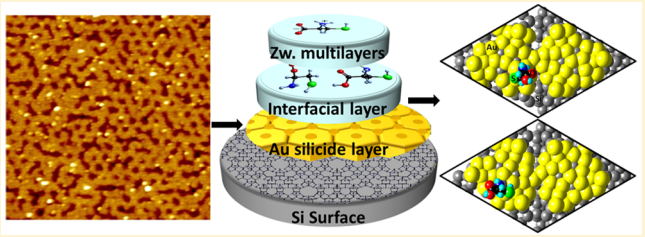

INTRODUCTION

Understanding the molecular interactions of multifunctional bio-organic molecules such as L-cysteine on a single-crystal metallic or semiconductor solid surface is important to developing practical applications not only in biosensors and biomolecular electronic devices, but also in drug delivery and diagnostic systems. As one of two principal sulfur-containing amino acids that are incorporated into proteins, cysteine is especially interesting because it contains three functional groups: amino ($-NH_2$), carboxylic acid (−COOH), and thiol (−SH) groups, which provide a wide variety of bonding possibilities and configurations with the surface and/or with other adsorbates. The interest in cysteine adsorption on single-crystal metal surfaces (e.g., Au,[1−10] Ag,[11,12] and Cu[1,13]) stems from their importance in bioanalytical, surface patterning, and molecular electronics.[14−16] Cysteine was found to normally bind to the metal (Au, Ag) in the form of a thiolate through the thiol group.[1,2,11,17] Depending on the nature of the surface, the two remaining functional groups, i.e., amino and carboxylic acid groups, could play an important role in attaching this trifunctional molecule to the surface,[18] and/or to other molecules. In contrast, investigation of cysteine adsorption on a semiconductor surface has been limited.[18−20] In our recent work on L-cysteine on one of the most popular benchmark semiconductor surfaces,[18] Si(111)7×7 surface,[21] we observe a "universal" three-stage growth process for cysteine, from interfacial to transitional to zwitterionic layers. Interestingly, the transitional layer is not usually found for the film growth of organic molecules on single-crystal metal surfaces.

In addition to bio/organic molecules, the 7×7 surface with directional dangling bonds also provides an important substrate for a wide range of inorganic materials, from gold and other metals to inorganic adsorbates, to fabricate supported metal clusters and nanostructures. These supported metal clusters and nanostructures provide stable nano-assemblies to study their interactions with biomolecules, promising new insight into processes occurring on catalysts and biosensors. To date, studies of biomolecular interaction with supported metallic nanostructures have remained particularly challenging and limited, due in part to the difficulties in preparing well-defined metallic nanostructures supported on a semiconductor surface. Only one notable study on "coadsorption" of Au and L-cysteine on rutile TiO_2(110) has been reported.[22] When L-cysteine was exposed to this wide-bandgap semiconductor surface first before the Au deposition, cysteine served as a linker molecule, and the formation of Au clusters was found to be smaller by a factor of 2−3 than those obtained by Au deposition followed by cysteine. In this latter case, cysteine was found to interact with both the gold deposits and the substrate surface through the thiol group with formation of S−Au and S−Ti bonds, respectively.

Received: April 24, 2018
Revised: May 30, 2018
Published: June 20, 2018

DOI: 10.1021/acs.jpcc.8b03877
J. Phys. Chem. C 2018, 122, 16113−16121

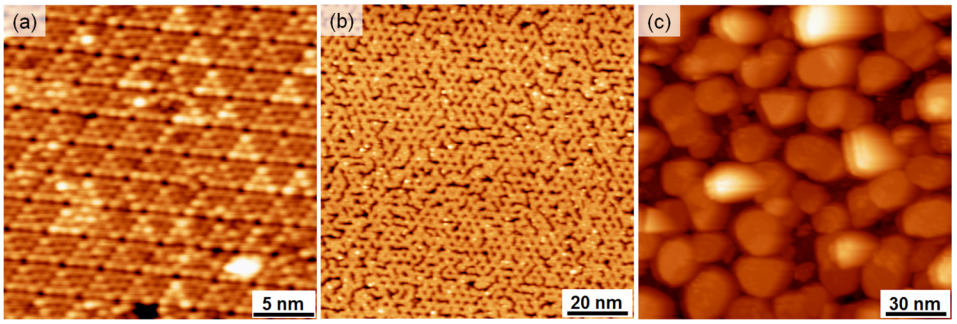

Figure 1. Filled-state STM images of (a) 0.004, (b) 0.76, and (c) 3.97 ML of Au on Si(111)7×7 surface at room temperature, all collected with a sample bias of −2.0 V and a tunneling current of 0.2 nA. The fields of view for (a), (b), and (c) are 25×25 nm^2, 100×100 nm^2, and 150×150 nm^2, respectively.

Here, we present the first investigation of the interactions of L-cysteine with a unique gold honeycomb nanonetwork on Si(111)7×7 surface and compare with those at low Au coverage (Au monomers and dimers) and high Au coverage (Au nanocrystallite film), all at room temperature. This supported gold honeycomb is particularly interesting because it represents a well-defined ultrathin two-dimensional (2D) semimetallic nanomaterial.

EXPERIMENTAL AND COMPUTATIONAL DETAILS

The experiments were performed in a custom-built five-chamber ultrahigh vacuum system (Omicron Nanotechnology, Inc.) with a base pressure lower than 5×10^{-11} mbar. The analysis chamber was equipped with a variable-temperature scanning probe microscope for atomic-resolution scanning tunneling microscopy (STM) imaging, and a high-performance spectrometer consisting of a monochromatized Al Kα source (1486.7 eV photon energy), a SPHERA hemispherical electron analyzer (operated with a pass energy of 20 eV), and a 7-channeltron detector assembly for X-ray photoelectron spectroscopy (XPS) analysis. The 7×7 reconstruction of a n-type Si(111) sample (2×11 mm^2, 0.3 mm thick, and with 0.005 Ω cm resistivity) was obtained by passing a direct current to flash-anneal the sample to ∼1200 °C for 10 s, followed by slow cooling to room temperature. This procedure produced large terraces of 7×7 reconstruction, as observed by STM. All STM images were obtained at room temperature using a sharp, electrochemically etched W tip and a constant tunneling current of 0.2 nA with appropriate sample bias voltages (negative bias for filled-state imaging and positive bias for empty-state imaging). To obtain the various Au nanoassemblies on the Si(111)7×7 surface, the clean 7×7 substrate was transferred to a molecular beam epitaxy growth chamber, in which Au (99.9999% purity, Alfa Aesar) was deposited by thermal evaporation at 1040 °C with the 7×7 substrate held at room temperature. Appropriate doses of Au were exposed to a freshly prepared 7×7 surface as described above to produce (a) Au monomers and dimers (nanoclusters), (b) Au honeycomb nanonetwork, and (c) Au nanocrystallite film.[23] After each exposure, both STM and XPS measurements were performed on the same supported Au nanoassembly in the analysis chamber. Each of the supported Au nanoassemblies was then introduced to the organic molecular beam epitaxy chamber to be exposed to L-cysteine using a low-temperature organic effusion cell (Dr. Ebert MBE-Komponenten GmbH). Cysteine (99.5% purity, Fluka), with a normal melting point at 240 °C, was deposited on the substrate with the effusion cell held at 140 °C[24] and the deposition chamber pressure at 2×10^{-9} mbar. The cysteine powders in the effusion cell were outgassed thoroughly overnight prior to the deposition. The molecular identity and integrity of cysteine during exposure were confirmed by their cracking patterns, collected in situ with a quadrupole mass spectrometer (Stanford Research System RGA-300), and found to be in good accord with the literature.[25] The amount of exposure time was used here to indicate the relative amount of cysteine deposition.[18] After the cysteine exposure on the Si surface, XPS spectra of the Si 2p, Au 4f, N 1s, C 1s, O 1s, and S 2s regions were recorded with an energy resolution of 0.7 eV full width at half-maximum (for the Ag $3d_{5/2}$ photoline at 368.3 eV). It should be noted that we have chosen to use the S 2s spectrum for quantification because the S 2p feature partially overlaps with one of the Si plasmon peaks located at ∼168.0 eV.[26] The spectra were fitted with Gaussian−Lorentzian lineshapes (70% Gaussian and 30% Lorentzian) along with the Shirley background using the Casa-XPS software, and the binding energies were referenced to the Si $2p_{3/2}$ peak of bulk Si at 99.3 eV.

Using large-scale ab initio quantum-mechanical calculations, based on the density functional theory (DFT) with van der Waals corrections (D2),[27] we provide precise structural models and adsorption energies for cysteine adspecies on the gold honeycomb nanonetwork supported on Si(111)7×7 surface. A $Si_{200}H_{49}$ slab employing the dimer-adatom-stacking fault (DAS) model is used to represent the pristine Si(111)7×7 surface,[21,28] while a $Au_{25}Si_6$ cluster is used to model one of six equivalent 7×7 half unit cells (around a corner hole) making up a hexagon cell in the gold honeycomb structure, where the six Si atoms correspond to the top layer atoms of the half unit cell (Figure S1).[23] The first-principle total energy calculations were performed within the generalized gradient approximation,[29,30] as defined by Perdew, Burke, and Ernzerhof (GGA-PBE),[31] and were based on the exchange-correlation functional and projector augmented-wave (PAW) potentials[32,33] to describe the effect of core electrons on the valence shells together with a plane-wave basis set used to span the valence electronic states. The Vienna Ab-initio Simulation Package[34−37] (VASP, version 5.4) with the MedeA platform (Materials Design, version 2.18) was used. The plane-wave expansion cutoff energy was set to 400 eV, and the surface Brillouin zone was sampled at the Γ point with k-point spacing of 0.5 $Å^{-1}$. Conjugate-gradient algorithm was employed to optimize the geometry of the atomic structure, and all Si atoms were completely relaxed until the forces on all the atoms were less than 0.02 eV/Å. The energy convergence of the self-

DOI: 10.1021/acs.jpcc.8b03877
J. Phys. Chem. C 2018, 122, 16113−16121

consistent field was set to 1.0×10^{-5} eV, with Methfessel-Paxton smearing of 0.2 eV.

RESULTS AND DISCUSSION

The STM images of three Au nanoassemblies obtained with appropriate exposures on Si(111)7×7: clusters (0.004 ML) [where 1 monolayer (ML) corresponds to 7.83×10^{14} atoms/cm^2 assuming the Si atomic density of an unreconstructed Si(111) surface], honeycomb nanonetwork (0.76 ML), and nanocrystallite film (3.97 ML) are shown in Figure 1.[23] Briefly, at the lowest Au coverage, there are only "sextet" and "triad" features located, respectively, on the faulted and unfaulted half unit cells, and these features correspond to individual Au adatoms translocating among, respectively, all six adatoms and three center adatom sites. There are also "scribble" features that correspond to a fast-moving Au dimer within a half unit cell. Further increase in the Au coverage to 0.76 ML leads to the formation of a complete gold silicide layer with the honeycomb nanonetwork covering the entire 7×7 unit cell except for the corner holes. This new gold nanonetwork, in effect, represents a 2D template of nanopores (with pore size of ~1 nm dia) that could be used for molecular trapping and nanotemplating applications. It also offers a new ultrathin conducting phase of fundamental interest to silicon device fabrication and to other applications in biofunctionalization. The presence of gold silicide has been observed for coverage up to ~2 ML (Figure 2a).[23] At a higher coverage of 3.97 ML, a thin film of Au nanocrystallites exhibiting regular triangular and polygonal faces, likely the (111) planes, is observed (Figure 1c).[23] The corresponding chemical-state compositions for specific Au coverages have been determined in our recent XPS study and are summarized in Figure 2a. Evidently, the spectra are dominated by a prominent Au $4f_{7/2}$ ($4f_{5/2}$) peak near 84.5 eV (88.1 eV) and 84.7 eV (88.3 eV) for clusters (0.004 ML) and honeycomb nanonetwork (0.76 ML), respectively, attributed to gold silicide. A second Au $4f_{7/2}$ ($4f_{5/2}$) feature emerged at 83.8 eV (87.4 eV) at higher Au coverage corresponds to metallic Au.[23] These three Au nanoassemblies are then used as the "supporting" substrates for investigating their interactions with cysteine. Before discussing the result for the supported gold honeycomb, we first present the cysteine adsorption data for the other nanoassemblies, representing the low-coverage and high-coverage limits of Au on Si(111)7×7.

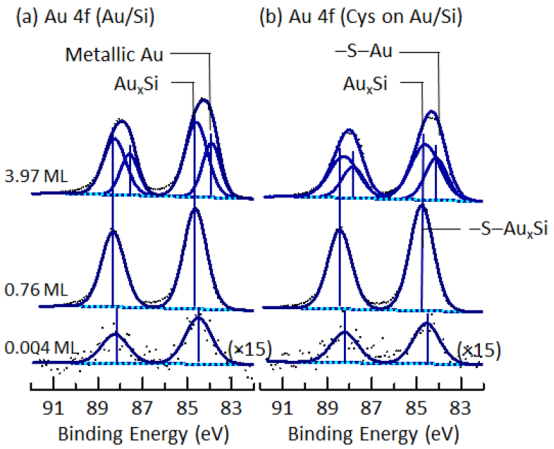

Figure 2. XPS spectra of the Au 4f region for three Au nanoassemblies obtained with coverages of 0.004, 0.76, and 3.97 ML on Si(111)7×7 at room temperature, (a) without and (b) with 20 min postexposure of cysteine.

Interaction of Cysteine with Supported Gold Monomers and Dimers (0.004 ML) and with Gold Nanocrystallite Film (3.97 ML). Figure 3 shows the O 1s, N 1s, C 1s, and S 2s spectra of cysteine deposited at room temperature on 0.004 ML of Au supported on Si(111)7×7 surface as a function of cysteine exposure time, with their corresponding peak positions and assignments of the fitted features given in Table S1. The corresponding filled-state STM image for this supported Au monomers and dimers (Figure 1a) shows a very low surface density of Au adatoms with the majority of the 7×7 reconstruction remaining clearly visible. We therefore expect that the cysteine growth evolution should closely follow that on a pristine Si(111)7×7 surface, but with some added contribution due to the presence of Au monomers and dimers. Not surprisingly, we observe three-stage growth process for cysteine, from the chemisorbed interfacial layer (first stage, 0.5−1.5 min) to the transitional layer (second stage, 4.5−60 min) and to zwitterionic multilayer film (third stage, 150 min). The coexistence of the N 1s feature at 398.8 eV (Figure 3b) and the S 2s feature at 227.1 eV (Figure 3d) at the lowest exposure (0.5 min), attributed to N−Si and S−Si bonds, respectively, indicates unidentate and/or bidentate bonding arrangements of cysteine at the interfacial layer through the respective N−H and S−H dissociative chemisorption on the 7×7 surface. The second N 1s feature that emerged at a higher binding energy upon higher exposures (1.5 min and above) is in good accord with the presence of the O−H···N hydrogen bond at 401.1 eV (Figure 3b) (where we use the triple-dot line "···" to denote a H-bond). This feature therefore confirms the formation of interlayer H-bond between a free carboxylic acid group of cysteine in the interfacial layer (first adlayer) and a free amino group of cysteine in the transitional layer (second adlayer).[38] Furthermore, the best fit for the C 1s spectrum (Figure 3c) is obtained by attributing four fitted peaks, located from low to high binding energy, to the $-CH_2-S-Si$, $-CH_2-SH$, $-CH-NH-Si$, and $-COOH$ moieties. The relative area ratios of 1:1:1:1 for these C 1s features found for 0.5−1.5 min exposure are consistent with the stoichiometric ratios expected for the first adlayer bonding. As the exposure increases into the transitional layer and zwitterionic multilayer regimes, the relative intensity of the $-CH_2-S-Si$ feature becomes reduced. Finally, the broad O 1s spectrum (Figure 3a) for exposure up to 60 min is consistent with the carbonyl component ($-C=O$) and hydroxyl oxygen ($-OH$).

The XPS spectra for the cysteine multilayer obtained at the 150 min exposure on the 7×7 surface pre-exposed with 0.004 ML of Au (Figure 3) are also found to be similar to those for cysteine multilayer on a pristine Si(111)7×7 surface.[18] The chemical shift of the O 1s feature for $-C=O/-OH$ at 532.6 eV to a lower binding energy can be attributed to a carboxylate group ($-COO^-$), while the appearance of a new N 1s feature at a higher binding energy (401.7 eV) corresponds to a protonated amino group ($-NH_3^+$). These new features affirm the formation of zwitterionic structure in the multilayer ($NH_3^+CHCH_2SHCOO^-$). The weaker intensity of the $-NH-$Si N 1s feature at 398.8 eV for the 150 min exposure than those for 1.5−60 min exposures (Figure 3b) suggests that the thickness of the zwitterionic layer has exceeded the photoelectron escape depth. Furthermore, the S 2s peak at 228.4 eV corresponds to an intact thiol group (Figure 3d), similar to

DOI: 10.1021/acs.jpcc.8b03877
J. Phys. Chem. C 2018, 122, 16113−16121

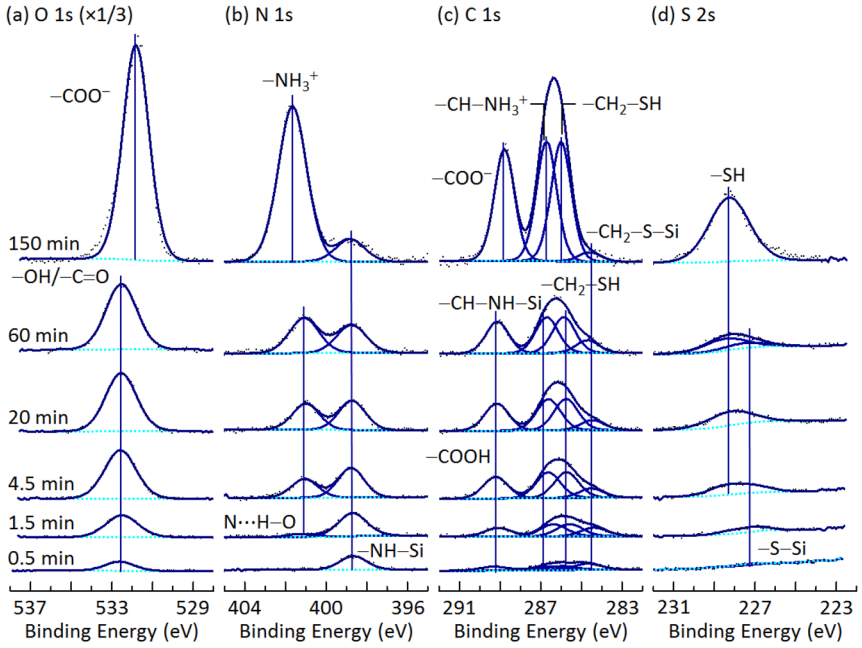

Figure 3. XPS spectra of (a) O 1s, (b) N 1s, (c) C 1s, and (d) S 2s regions of L-cysteine deposited on Au(0.004 ML)/Si(111)7×7 as a function of cysteine exposure time.

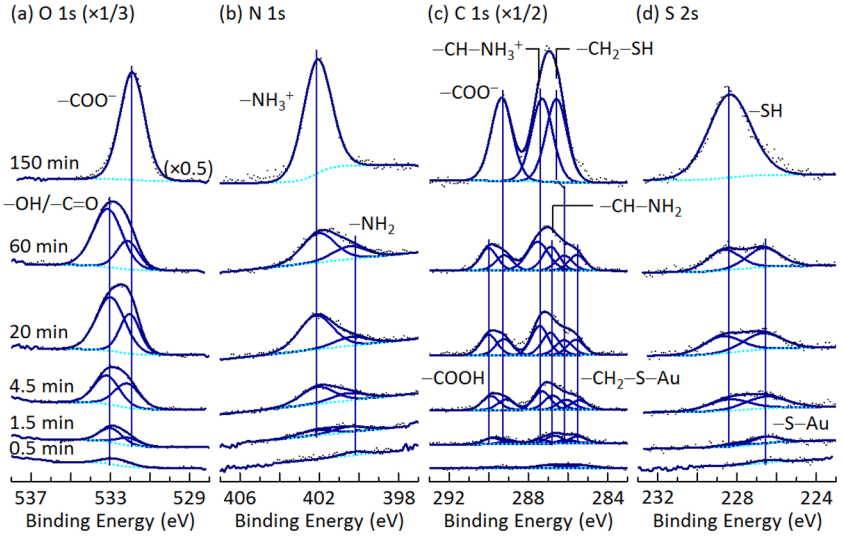

Figure 4. XPS spectra of (a) O 1s, (b) N 1s, (c) C 1s, and (d) S 2s regions of L-cysteine deposited on Au(3.97 ML)/Si(111)7×7 as a function of cysteine exposure time.

those observed for cysteine powder and a multilayer cysteine film on a pristine Si(111)7×7 surface.[18] The corresponding C 1s spectrum (Figure 3c) consists of a broad band centered at 286.4 eV, attributable to the three alkyl carbons in $-CH_2-S-$Si, (at 284.6 eV), $-CH_2-SH$ (at 286.0 eV), and $-CH-NH_3^+$ (at 286.7 eV), and a weaker feature at 288.8 eV corresponding to the carboxylate group. We also obtain the Au 4f spectra for a 20 min cysteine exposure deposited on Si(111)7×7 predeposited with 0.004 ML of Au (Figure 2b). The presence of cysteine appears to cause only a 0.1 eV shift in the Au $4f_{7/2}$ peak to a higher binding energy (84.6 eV), when compared to the corresponding pristine supported Au nanoassembly shown in Figure 2a.

Figure 4 shows the O 1s, N 1s, C 1s, and S 2s spectra of cysteine deposited at room temperature on a Au nanocrystallite film supported on Si(111)7×7 surface as a function of cysteine exposure time, with their corresponding peak positions and assignments of the fitted features given in Table S2. The filled-state STM image (Figure 1c) shows the Au nanocrystallites with their regular triangular and polygonal faces [likely the (111) plane] exposed, reflecting their single-crystalline nature. With 3.97 ML of Au coverage, there is no sign of any 7×7 registry from the reconstructed Si(111) substrate. As the thiol group is known to interact strongly with noble metals (Au, Ag, Cu) and binds to them in the form of thiolate,[1,2,11,17] there is no evidence of any three-stage growth process (Figure 4). At the lowest exposure (0.5 min), the S 2s peak at 226.6 eV and the N 1s peak at 400.1 eV indicate attachment of cysteine to Au via a thiolate group and leaving the amino group free. The corresponding O 1s feature consists mainly of a broad peak at 533.0 eV, which can be attributed to unattached $-C{=}O$ and $-OH$. This further confirms that L-

DOI: 10.1021/acs.jpcc.8b03877
J. Phys. Chem. C 2018, 122, 16113−16121

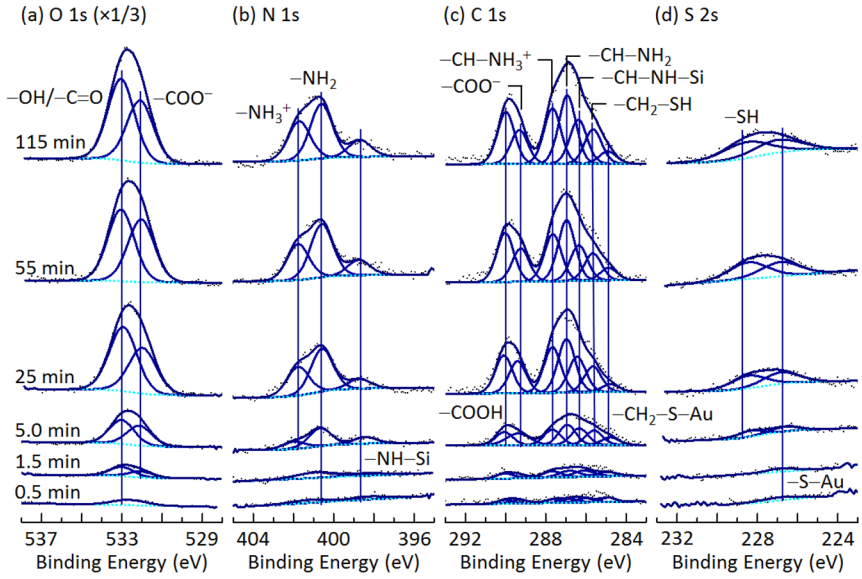

Figure 5. XPS spectra of (a) O 1s, (b) N 1s, (c) C 1s, and (d) S 2s regions of L-cysteine deposited on Au(0.76 ML)/Si(111)7×7 as a function of cysteine exposure time.

cysteine chemisorbs at room temperature via the sulfur atom on the supported Au nanocrystallites. With increasing exposure to 1.5−60 min, we observe the emergence of additional features for O 1s at 532.1 eV (Figure 4a), N 1s at 402.0 eV (Figure 4b), and S 2s at 228.2 eV (Figure 4d), which correspond to carboxylate group ($-COO^-$), protonated amino group ($-NH_3^+$), and intact thiol group (−SH), respectively. The corresponding C 1s spectra have been fitted with six components, from low to high binding energy, consistent with assignment to the $-CH_2-S-Au$, $-CH_2-SH$, $-CH-NH_2$, $-CH-NH_3^+$, $-COO^-$, and COOH moieties, respectively. When the coverage of cysteine is increased above a monolayer, cysteine molecules are expected to physisorb on top of the chemisorbed interfacial layer in the zwitterionic form with a protonated amino group and a carboxylate group.

Analogous to adsorption of L-cysteine on Ag(111) surface,[11] we find that for the multilayer (150 min) cysteine exposure, only a single strong broad S 2s peak at 228.3 eV is observed (Figure 4d), which indicates an intact thiol group. The single O 1s feature at 532.0 eV (Figure 4a) and N 1s feature at 402.1 eV (Figure 4b) are also consistent with the carboxylate and protonated amino groups, respectively, in the zwitterionic multilayer. The broad C 1s band at 287.0 eV is due to a combination of $-CH_2-SH$ and $-CH-NH_3^+$ moieties, while the well-resolved feature at 289.3 eV corresponds to the $-COO^-$ group (Figure 4c). We also observe discernible chemical shifts (∼0.2 eV) to a higher binding energy for both the gold silicide $4f_{7/2}$ peak at 84.9 eV and Au metallic $4f_{7/2}$ peak at 84.1 eV after 20 min cysteine deposition on the Au nanocrystallite film (Figure 2b), when compared to the respective Au 4f features for the pristine Au nanoassemblies. These small chemical shifts are due to their sulfur to Au interaction and confirm the reducing nature of the thiolate moiety.

Interaction of Cysteine with Supported Gold Honeycomb Nanonetworks (0.76 ML). In contrast to the supported gold nanoassemblies at the low Au coverage limit (i.e., monomers and dimers) and high Au coverage limit (i.e., nanocrystallite film), the supported gold honeycomb nanonetworks offer discernibly well-ordered biocompatible templates for functionalization with bio/organic molecules. Figure 5 shows the XPS spectra of cysteine deposited at on a supported gold honeycomb nanonetwork as a function of cysteine exposure time, with their corresponding peak positions and assignments of the fitted features given in Table S3.

At the very low exposures of 0.5−1.5 min, the S 2s spectra (Figure 5d) show only one weak peak, assigned to the −S−Au bond, while the N 1s spectra (Figure 5b) reveal two weak peaks at 398.5 and 400.4 eV, attributed to −NH−Si and $-NH_2$, respectively.[38] These features indicate the coexistence of two unidentate adspecies (in the interfacial layer) that involve bonding with Au atoms through the thiol group (−SH) and with Si atoms through the amino group ($-NH_2$). With increasing exposure above 5.0 min, we observe the emergence and growth of a new N 1s feature at 401.8 eV (Figure 5b), attributable to protonated amino group ($-NH_3^+$). The corresponding O 1s band centered at 533.0 eV (Figure 5a) consists of a stronger O 1s peak for the carbonyl group (−C═O) and hydroxyl group (−OH), and a weaker O 1s peak for the carboxylate group ($-COO^-$) at a lower binding energy. Furthermore, the S 2s feature at 228.3 eV for exposures above 5 min indicates the presence of an intact thiol group (Figure 5d), which confirms the existence of zwitterionic structures in the physisorbed layer. At the same time, there appears to be equal population of the −S−Au moiety even for the higher cysteine exposure, which suggests that the thickness of the zwitterionic layer has not exceeded the photoelectron escape depth. The C 1s spectra shown in Figure 5c can be fitted with seven C 1s components, which can be attributed, respectively from low to high binding energy, to $-CH_2-S-Au$, $-CH_2-SH$, −CH−NH−Si, $-CH-NH_2$, $-CH-NH_3^+$, $-COO^-$, and COOH. The absence of any XPS feature attributable to interlayer O−H···N H-bond at ∼401.0 eV supports that there is no transitional layer in the cysteine growth process on both Au (0.76 ML) and Au (3.97 ML) nanoassemblies. The complementary Au 4f spectrum for a 20 min exposure of cysteine to the gold honeycomb nanonetwork shown in Figure 2b indicates that the formation of S−Au bond has evidently shifted the gold-silicide Au $4f_{7/2}$ peak to a higher binding energy (84.9 eV) from 84.7 eV for a pristine gold honeycomb

DOI: 10.1021/acs.jpcc.8b03877
J. Phys. Chem. C 2018, 122, 16113−16121

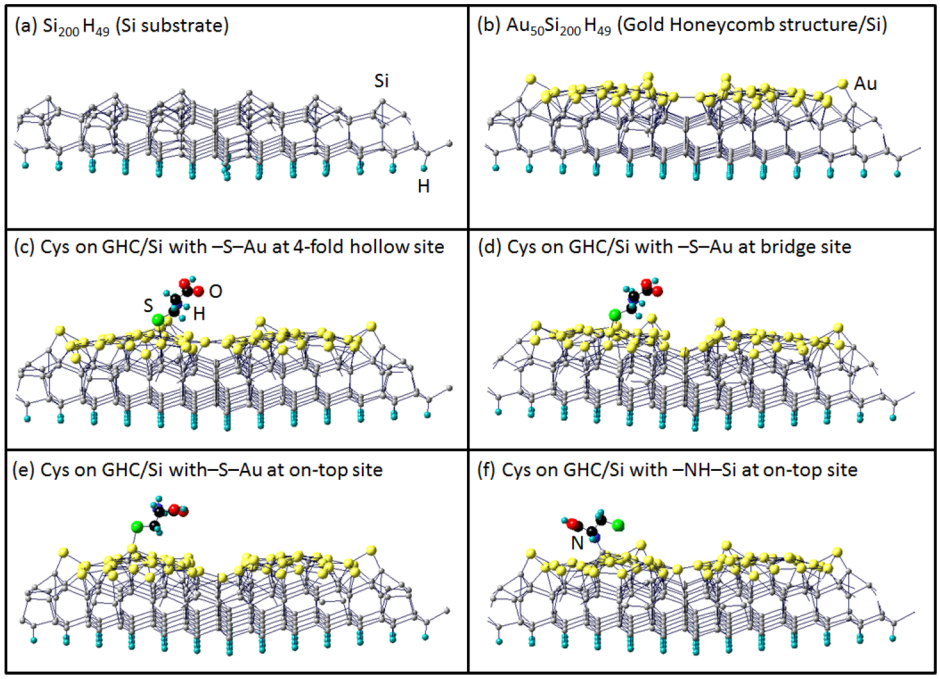

Figure 6. Perspective views of the equilibrium structures obtained from DFT-D2 calculations for (a) $Si_{200}H_{49}$ slab as a model pristine Si(111)7×7 surface; (b) $Au_{50}Si_{200}H_{49}$ cluster for one Si unit cell representing two of the six half-unit-cell segments of the gold honeycomb (GHC) unit in the gold silicide nanonetwork; 4-fold hollow and bridge adsorption configurations of cysteine adspecies between (c) four Au atoms and (d) two Au atoms, respectively; on-top configurations of cysteine adspecies on the supported gold honeycomb through (e) –S–Au bond and (f) –NH–Si bond.

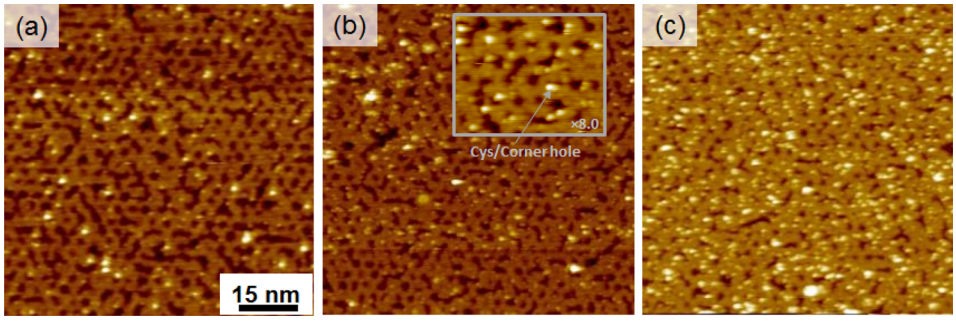

Figure 7. Filled-state STM images (75×75 nm^2), obtained with a sample bias of –2.0 V, for (a) 5 s, (b) 20 s, and (c) 65 s exposure of cysteine on gold honeycomb nanonetwork supported on Si(111)7×7 surface. Inset in (b) shows a magnified (8×) view of a cysteine adspecies at the nanopore (i.e., corner hole) Si site.

nanonetwork. This shift to a higher binding energy is consistent with cysteine interaction through the S–Au bonding that causes a more electron-withdrawing chemical environment that leads to a more positive Au ion core.

The filled-state STM image (Figure 1b) shows that the honeycomb nanonetwork is made up of six triangular Au clusters, interconnected to one another at the dimer rows of the Si(111)7×7 surface, around each empty corner hole leaving its directional dangling bond unoccupied. Our recent XPS study has demonstrated that the honeycomb nanonetwork exhibits the gold silicide chemical state.[23] Furthermore, our complementary DFT calculations show that the Au_9Si_3 structure (Figure S1b) is a possible nucleation center for one of the six segments of the honeycomb unit, with each segment consisting of 3 Au atoms located at the Si center adatom sites, 3 Au atoms located atop of the Si restatoms, and 3 Au atoms placed at the pedestal atom sites of the Si restatoms. In Figure 6b, we use a $Au_{50}Si_{200}H_{49}$ cluster to represent two of the six segments that make up an honeycomb unit on one 7×7 unit cell. Each segment involves direct bonding of Au atoms to 3 corner Si adatoms and to 3 pedestal atoms of the Si corner adatoms and center adatoms (Figure S1c). The Au atoms in these segments essentially make up the majority of the first gold silicide layer, with some of displaced Si center adatom sites exposed. The unoccupied dangling bonds on these displaced center adatom sites and on the corner holes could therefore offer plausible anchoring points for inorganic/biomolecules adspecies above the honeycomb nanonetwork.[23] In effect, the honeycomb serves as a "mask" to create a new Si dangling bond template, with different pitch spacing between the anchoring points, for surface functionalization.

Our DFT-D2 calculations of adsorbed cysteine on gold honeycomb supported on Si(111)7×7 surface show that the most favorable adsorption configuration corresponds to the cysteine adspecies bonding through the –S–Au bonds to four Au atoms at the 4-fold hollow site (Figure 6c). This is followed

DOI: 10.1021/acs.jpcc.8b03877
J. Phys. Chem. C 2018, 122, 16113–16121

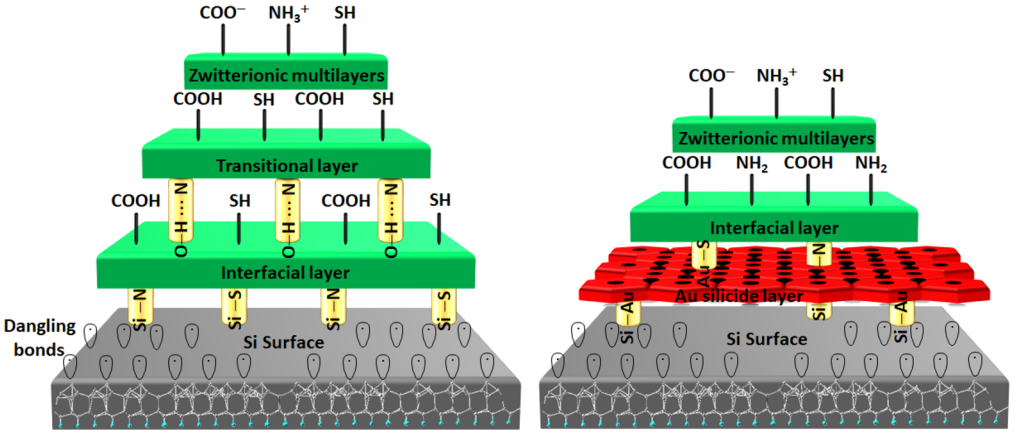

Figure 8. Schematic growth models involving available surface functional groups and plausible intralayer and interlayer hydrogen bonding interactions for L-cysteine adsorption on (left) Si(111)7×7 surface (following the universal three-stage growth on a semiconductor surface) and (right) gold-silicide honeycomb nanonetworks (following the two-stage growth commonly observed on a metal surface).

by cysteine bonding between two Au atoms at the bridge site (Figure 6d), and by cysteine bonding with a Au atom at the on-top site (center Au atom on the 7×7 half unit cell, Figure 6e), both through the formation of a S−Au bond, and finally by cysteine bonding through a −NH−Si bond at the Si adatom (with an unoccupied dangling bond, Figure 6f). The corresponding adsorption energies of these configurations are 2.84 eV (Figure 6f), 1.85 eV (Figure 6e), and 1.51 eV (Figure 6d) less negative than that for the 4-fold hollow site (Figure 6c). The gold honeycomb nanonetwork therefore represents a stable mask for cysteine (and other bio-organic) adsorbate, with simultaneous Au and Si bonding sites at well-defined interatomic pitch spacings and different reactivities. This template therefore provides a viable platform for constructing a hybrid nanoarchitecture consisting of smaller molecules surrounded by larger molecules.

Figure 7 shows typical filled-state STM images (75×75 nm^2) for three cysteine exposures on the supported gold honeycomb nanonetwork. In these STM images, brightened features on top of the honeycomb nanonetwork indicate cysteine adspecies, and their number density appears to increase with increasing cysteine exposure. Closer examination of these STM images reveals that the cysteine adspecies are anchored on both Au hexagonal grids (~4 nm wide) and nanopores (~1 nm dia.). Along with our XPS data (Figure 5), these STM results therefore confirm our bonding picture. This novel gold silicide honeycomb nanonetwork, with its 2D (ultrathin) template of nanopores, could offer a number of interesting applications for molecular trapping. The trapped molecules with appropriate functional groups can be used as linkers to create patterns of other organic adspecies.

In Figure 8, we compare schematically the bonding models involving different available surface functional groups for the growth evolution of cysteine on a Si(111)7×7 surface, without and with the supported gold honeycomb nanonetwork. For cysteine adsorption on the pristine Si(111)7×7 surface without and with the Au monomers and dimers, we observe the "universal" three-stage growth, with both Si−S and Si−N bonds providing the primary bonding for the interfacial layer. This is followed by the formation of a transitional layer through interlayer O−H···N hydrogen bonding, and finally by formation of the zwitterionic multilayers (Figure 8, left). For the gold honeycomb nanonetwork supported on the 7×7 surface, the interfacial layer of cysteine involves both the Au−S bond with the gold silicide honeycomb and Si−N bond with exposed Si sites. Much like the adsorption of cysteine on gold single crystal[4,6] and other metal single-crystal surfaces,[1,11,39] no transitional layer is observed and the zwitterionic multilayers immediately follow the interfacial layer growth (Figure 8, right). This is an important result because the formation of the ultrathin gold silicide layer (in the form of a honeycomb nanonetwork) has effectively converted the semiconductor surface to a metal-like surface. Given the biocompatibility of gold itself, appropriate functionalization of the supported gold honeycomb nanonetwork is of critical value to allow specific conjugation with targeted bio/organic moieties. The present work also illustrates that cysteine can be used as a versatile linker, with the availability of two free functional groups upon adsorption, to bridge between the Au template and incoming target molecules. Functionalization of the gold honeycomb nanonetwork by trifunctional molecules therefore offers an important strategy for developing chemical sensing, drug delivery and diagnostic systems.

CONCLUSION

The room-temperature growth evolution of cysteine on three gold nanoassemblies of increasing coverage from Au monomers and dimers to honeycomb nanonetwork to nanocrystallite film, supported on Si(111)7×7 surface has been studied by using a three-pronged approach that combines XPS and STM data with large-scale ab initio DFT-D2 calculations. The adsorption features in the adlayers are found to be strongly dependent on the nature of the interface region. For low Au coverage (0.004 ML) that decorates the Si(111)7×7 surface with minor populations of Au monomers and dimers, we observe a three-stage growth process of cysteine, similar to that found for a pristine 7×7 surface. For higher Au coverages, the absence of any N 1s feature at 401.0 eV that corresponds to interlayer O−H···N hydrogen bond affirms the lack of a transitional layer for cysteine adsorbed on the supported gold silicide honeycomb nanonetwork and Au nanocrystallite film. These results from both STM and XPS studies therefore support our hypothesis that this unique mask of gold silicide honeycomb nanonetwork, with its 2D template of nanopores, could offer a number of novel applications for selective multisize molecular trapping, with the bonding of unidentate adspecies on Si corner hole through the thiol group and a second unidentate adspecies of a different size on the Au

DOI: 10.1021/acs.jpcc.8b03877
J. Phys. Chem. C 2018, 122, 16113−16121

grids through the amino group. The capability of providing different functional groups free to interact with incoming chemical moieties offer additional flexibility in multispecies detection and monitoring based on formation of appropriate chemical bonds.

■ ASSOCIATED CONTENT

Supporting Information

The Supporting Information is available free of charge on the ACS Publications website at DOI: 10.1021/acs.jpcc.8b03877.

Equilibrium structures obtained by large-scale DFT-D2 calculations and XPS peak-fitting data (PDF)

■ AUTHOR INFORMATION

Corresponding Authors

*E-mail: tong@uwaterloo.ca (K.T.L.).
*E-mail: frahsepar@ut.ac.ir (F.R.R.).

ORCID

Kam Tong Leung: 0000-0002-1879-2806

Author Contributions

#F.R.R and K.T. L. contributed equally.

Notes

The authors declare no competing financial interest.

■ ACKNOWLEDGMENTS

This work was supported by the Natural Sciences and Engineering Research Council of Canada.

■ REFERENCES

(1) Uvdal, K.; Bodo, P.; Liedberg, B. L-Cysteine Adsorbed on Gold and Copper: An X-Ray Photoelectron Spectroscopy Study. *J. Colloid Interface Sci.* **1992**, *149*, 162−173.

(2) Kühnle, A.; Linderoth, T. R.; Hammer, B.; Besenbacher, F. Chiral Recognition in Dimerization of Adsorbed Cysteine Observed by Scanning Tunnelling Microscopy. *Nature* **2002**, *415*, 891−893.

(3) Kühnle, A.; Linderoth, T. R.; Besenbacher, F. Self-Assembly of Monodispersed, Chiral Nanoclusters of Cysteine on the Au(110)-(1×2) Surface. *J. Am. Chem. Soc.* **2003**, *125*, 14680−14681.

(4) Kühnle, A.; Linderoth, T. R.; Schunack, M.; Besenbacher, F. L-Cysteine Adsorption Structures on Au(111) Investigated by Scanning Tunneling Microscopy under Ultrahigh Vacuum Conditions. *Langmuir* **2006**, *22*, 2156−2160.

(5) Cossaro, A.; Terreni, S.; Cavalleri, O.; Prato, M.; Cvetko, D.; Morgante, A.; Floreano, L.; Canepa, M. Electronic and Geometric Characterization of the L-Cysteine Paired-Row Phase on Au(110). *Langmuir* **2006**, *22*, 11193−11198.

(6) Mateo-Martí, E.; Rogero, C.; Gonzalez, C.; Sobrado, J. M.; de Andrés, P. L.; Martin-Gago, J. A. Interplay between Fast Diffusion and Molecular Interaction in the Formation of Self-Assembled Nanostructures of S-Cysteine on Au(111). *Langmuir* **2010**, *26*, 4113−4118.

(7) Kühnle, A. Self-Assembly of Organic Molecules at Metal Surfaces. *Curr. Opin. Colloid Interface Sci.* **2009**, *14*, 157−168.

(8) Xu, Q.-M.; Wan, L.-J.; Wang, C.; Bai, C.-L.; Wang, Z.-Y.; Nozawa, T. New Structure of L-Cysteine Self-Assembled Monolayer on Au(111): Studies by In Situ Scanning Tunneling Microscopy. *Langmuir* **2001**, *17*, 6203−6206.

(9) Cavalleri, O.; Gonella, G.; Terreni, S.; Vignolo, M.; Floreano, L.; Morgante, A.; Canepa, M.; Rolandi, R. High Resolution X-Ray Photoelectron Spectroscopy of L-Cysteine Self-Assembled Films. *Phys. Chem. Chem. Phys.* **2004**, *6*, 4042−4046.

(10) Gonella, G.; Terreni, S.; Cvetko, D.; Cossaro, A.; Mattera, L.; Cavalleri, O.; Rolandi, R.; Morgante, A.; Floreano, L.; Canepa, M. Ultrahigh Vacuum Deposition of L-Cysteine on Au(110) Studied by High-Resolution X-Ray Photoemission: From Early Stages of Adsorption to Molecular Organization. *J. Phys. Chem. B* **2005**, *109*, 18003−18009.

(11) Fischer, S.; Papageorgiou, A. C.; Marschall, M.; Reichert, J.; Diller, K.; Klappenberger, F.; Allegretti, F.; Nefedov, A.; Woll, C.; Barth, J. V. L-Cysteine on Ag(111): A Combined STM and X-Ray Spectroscopy Study of Anchorage and Deprotonation. *J. Phys. Chem. C* **2012**, *116*, 20356−20362.

(12) Santos, E.; Avalle, L. B.; Scurtu, R.; Jones, H. L-Cysteine Films on Ag(111) Investigated by Electrochemical and Nonlinear Optical Methods. *Chem. Phys.* **2007**, *342*, 236−244.

(13) Thomsen, L.; Wharmby, M. T.; Riley, D. P.; Held, G.; Gladys, M. J. The Adsorption and Stability of Sulfur Containing Amino Acids on Cu{531}. *Surf. Sci.* **2009**, *603*, 1253−1261.

(14) Vallee, A.; Humblot, V.; Pradier, C.-M. Peptide Interactions with Metal and Oxide Surfaces. *Acc. Chem. Res.* **2010**, *43*, 1297−1306.

(15) Chi, Q.; Zhang, J.; Nielsen, J. U.; Friis, E. P.; Chorkendorff, I.; Canters, G. W.; Andersen, J. E. T.; Ulstrup, J. Molecular Monolayers and Interfacial Electron Transfer of Pseudomonas Aeruginosa Azurin on Au(111). *J. Am. Chem. Soc.* **2000**, *122*, 4047−4055.

(16) Gerster, D.; Reichert, J.; Bi, H.; Barth, J. V.; Kaniber, S. M.; Holleitner, A. W.; Visoly-Fisher, I.; Sergani, S.; Carmeli, I. Photocurrent of a Single Photosynthetic Protein. *Nat. Nanotechnol.* **2012**, *7*, 673−676.

(17) Schreiber, F. Structure and Growth of Self-Assembling Monolayers. *Prog. Surf. Sci.* **2000**, *65*, 151−256.

(18) Rahsepar, F. R.; Zhang, L.; Farkhondeh, H.; Leung, K. T. Biofunctionalization of Si(111)7×7 by "Renewable" L-Cysteine Transitional Layer. *J. Am. Chem. Soc.* **2014**, *136*, 16909−16918.

(19) Ataman, E.; Isvoranu, C.; Knudsen, J.; Schulte, K.; Andersen, J. N.; Schnadt, J. Adsorption of L-Cysteine on Rutile TiO2(110). *Surf. Sci.* **2011**, *605*, 179−186.

(20) Huang, J. Y.; Ning, Y. S.; Yong, K. S.; Cai, Y. H.; Tang, H. H.; Shao, Y. X.; Alshahateet, S. F.; Sun, Y. M.; Xu, G. Q. Binding of Glycine and L-Cysteine on Si(111)-7×7. *Langmuir* **2007**, *23*, 6218−6226.

(21) Takayanagi, K.; Tanishiro, Y.; Takahashi, M.; Takahashi, S. Structural Analysis of Si(111)7×7 by UHV Transmission Electron Diffraction and Microscopy. *J. Vac. Sci. Technol., A* **1985**, *3*, 1502−1506.

(22) Ataman, E.; Isvoranu, C.; Knudsen, J.; Schulte, K.; Andersen, J. N.; Schnadt, J. Modification of the Size of Supported Clusters by Coadsorption of an Organic Compound: Gold and L-Cysteine on Rutile TiO2(110). *Langmuir* **2011**, *27*, 11466−11474.

(23) Rahsepar, F. R.; Zhang, L.; Leung, K. T. Two-Dimensional Self-Assembled Gold Silicide Honeycomb Nanonetwork on Si(111)7×7. *J. Phys. Chem. C* **2014**, *118*, 9051−9055.

(24) Gross, D.; Grodsky, G. On the Sublimation of Amino Acids and Peptides. *J. Am. Chem. Soc.* **1955**, *77*, 1678−1680.

(25) Naumkin, A. V.; Kraut-Vass, A.; Gaarenstroom, S. W.; Powell, C. J. X-Ray Photoelectron Spectroscopy Database. In *NIST Chemistry Webbook*; Linstrom, P. J.; Mallard, W. G., Eds.; NIST Standard Reference Database 20, Version 4.1; National Institute of Standards and Technology: Gaithersburg, MD; http://webbook.nist.gov (accessed September 15, 2012).

(26) He, J.; Patitsas, S. N.; Preston, K. F.; Wolkow, R. A.; Wayner, D. D. M. Covalent Bonding of Thiophenes to Si(111) by a Halogenation/thienylation Route. *Chem. Phys. Lett.* **1998**, *286*, 508−514.

(27) Grimme, S. Semiempirical GGA-Type Density Functional Constructed with a Long-Range Dispersion Correction. *J. Comput. Chem.* **2006**, *27*, 1787−1799.

(28) Takayanagi, K.; Tanishiro, Y.; Takahashi, S.; Takahashi, M. Structure Analysis of Si(111)-7×7 Reconstructed Surface by Transmission Electron Diffraction. *Surf. Sci.* **1985**, *164*, 367−392.

(29) Wang, Y.; Perdew, J. P. Correlation Hole of the Spin-Polarized Electron Gas, with Exact Small-Wave-Vector and High-Density Scaling. *Phys. Rev. B: Condens. Matter Mater. Phys.* **1991**, *44*, 13298−13307.

(30) Perdew, J. P.; Chevary, J. A.; Vosko, S. H.; Jackson, K. A.; Pederson, M. R.; Singh, D. J.; Fiolhais, C. Atoms, Molecules, Solids, and Surfaces: Applications of the Generalized Gradient Approximation for Exchange and Correlation. *Phys. Rev. B: Condens. Matter Mater. Phys.* **1992**, *46*, 6671−6687.
(31) Perdew, J. P.; Burke, K.; Ernzerhof, M. Generalized Gradient Approximation Made Simple. *Phys. Rev. Lett.* **1996**, *77*, 3865−3868.
(32) Blochl, P. E. Projector Augmented-Wave Method. *Phys. Rev. B: Condens. Matter Mater. Phys.* **1994**, *50*, 17953−17979.
(33) Kresse, G.; Joubert, D. From Ultrasoft Pseudopotentials to the Projector Augmented-Wave Method. *Phys. Rev. B: Condens. Matter Mater. Phys.* **1999**, *59*, 1758−1775.
(34) Kresse, G.; Hafner, J. Ab Initio Molecular Dynamics for Liquid Metals. *Phys. Rev. B: Condens. Matter Mater. Phys.* **1993**, *47*, 558−561.
(35) Kresse, G.; Hafner, J. Ab Initio Molecular-Dynamics Simulation of the Liquid-Metal—amorphous-Semiconductor Transition in Germanium. *Phys. Rev. B: Condens. Matter Mater. Phys.* **1994**, *49*, 14251−14269.
(36) Kresse, G.; Furthmuller, J. Efficient Iterative Schemes for Ab Initio Total-Energy Calculations Using a Plane-Wave Basis Set. *Phys. Rev. B: Condens. Matter Mater. Phys.* **1996**, *54*, 11169−11186.
(37) Kresse, G.; Furthmuller, J. Efficiency of Ab-Initio Total Energy Calculations for Metals and Semiconductors Using a Plane-Wave Basis Set. *Comput. Mater. Sci.* **1996**, *6*, 15−50.
(38) Rahsepar, F. R.; Moghimi, N.; Leung, K. T. Surface-Mediated Hydrogen Bonding of Proteinogenic α-Amino Acids on Silicon. *Acc. Chem. Res.* **2016**, *49*, 942−951.
(39) Mateo Marti, E.; Methivier, C.; Pradier, C. M. (S)-Cysteine Chemisorption on Cu110, from the Gas or Liquid Phase: An FT-RAIRS and XPS Study. *Langmuir* **2004**, *20*, 10223−10230.

DOI: 10.1021/acs.jpcc.8b03877
J. Phys. Chem. C 2018, 122, 16113−16121